ACS NANO

www.acsnano.org

Parrotfish Teeth: Stiff Biominerals Whose Microstructure Makes Them Tough and Abrasion-Resistant To Bite Stony Corals

Matthew A. Marcus,[*,†,#] Shahrouz Amini,[‡,#] Cayla A. Stifler,[§] Chang-Yu Sun,[§] Nobumichi Tamura,[†] Hans A. Bechtel,[†] Dilworth Y. Parkinson,[†] Harold S. Barnard,[†] Xiyue X. X. Zhang,[†] J. Q. Isaiah Chua,[‡] Ali Miserez,[‡,∥] and Pupa U. P. A. Gilbert[*,§,⊥,∇]

[†]Advanced Light Source, Lawrence Berkeley Laboratory, Berkeley, California 94720, United States

[‡]Biological and Biomimetic Material Laboratory, School of Materials Science and Engineering, Nanyang Technological University, 637553 Singapore

[§]Department of Physics, University of Wisconsin−Madison, Madison, Wisconsin 53706, United States

[∥]School of Biological Sciences, Nanyang Technological University, 637551 Singapore

[⊥]Departments of Chemistry, Geoscience, Materials Science Program, University of Wisconsin−Madison, Madison, Wisconsin 53706, United States

Supporting Information

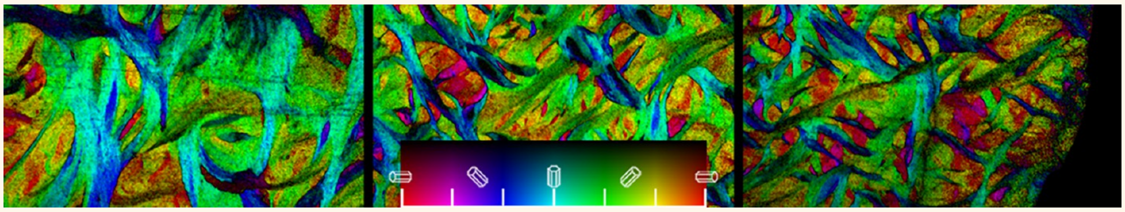

ABSTRACT: Parrotfish (*Scaridae*) feed by biting stony corals. To investigate how their teeth endure the associated contact stresses, we examine the chemical composition, nano- and microscale structure, and the mechanical properties of the steephead parrotfish *Chlorurus microrhinos* tooth. Its enameloid is a fluorapatite ($Ca_5(PO_4)_3F$) biomineral with outstanding mechanical characteristics: the mean elastic modulus is 124 GPa, and the mean hardness near the biting surface is 7.3 GPa, making this one of the stiffest and hardest biominerals measured; the mean indentation yield strength is above 6 GPa, and the mean fracture toughness is ~2.5 MPa·m$^{1/2}$, relatively high for a highly mineralized material. This combination of properties results in high abrasion resistance. Fluorapatite X-ray absorption spectroscopy exhibits linear dichroism at the Ca L-edge, an effect that makes peak intensities vary with crystal orientation, under linearly polarized X-ray illumination. This observation enables polarization-dependent imaging contrast mapping of apatite, a method to quantitatively measure and display nanocrystal orientations in large, pristine arrays of nano- and microcrystalline structures. Parrotfish enameloid consists of 100 nm-wide, microns long crystals co-oriented and assembled into bundles interwoven as the warp and the weave in fabric and therefore termed fibers here. These fibers gradually decrease in average diameter from 5 μm at the back to 2 μm at the tip of the tooth. Intriguingly, this size decrease is spatially correlated with an increase in hardness.

KEYWORDS: *nanomechanics, enameloid, enamel, biter, photoemission electron microscopy (PEEM), mesocrystal, PIC mapping*

Parrotfish are a diverse family of fish (Figure 1A), which specialize in biting corals, to eat their polyps and symbionts,[4] and excreting the ground-up coral skeleton, which then significantly contributes to the white sand beaches characteristic of tropical islands.[5] Erosion of coral by parrotfish occurs at a rate comparable not only to the rates at which other bioeroders, such as sea urchins and chitons, remove material but also to the rate at which coral skeletons grow.[6] Parrotfish therefore play a significant role in reef ecosystems. There is evidence from core samples that declines in coral abundance were driven by declines in parrotfish abundance in the last 3000 years.[7] These fish have two sets of teeth, for two separate functions: a beak for biting corals (Figures 1A) and a pharyngeal mill for grinding and chewing the bitten-off coral, so organics can be absorbed. The specialized biting beak, studied here, includes two upper dental plates and two lower

Received: July 17, 2017
Accepted: October 20, 2017
Published: October 20, 2017

DOI: 10.1021/acsnano.7b05044
ACS Nano 2017, 11, 11856−11865

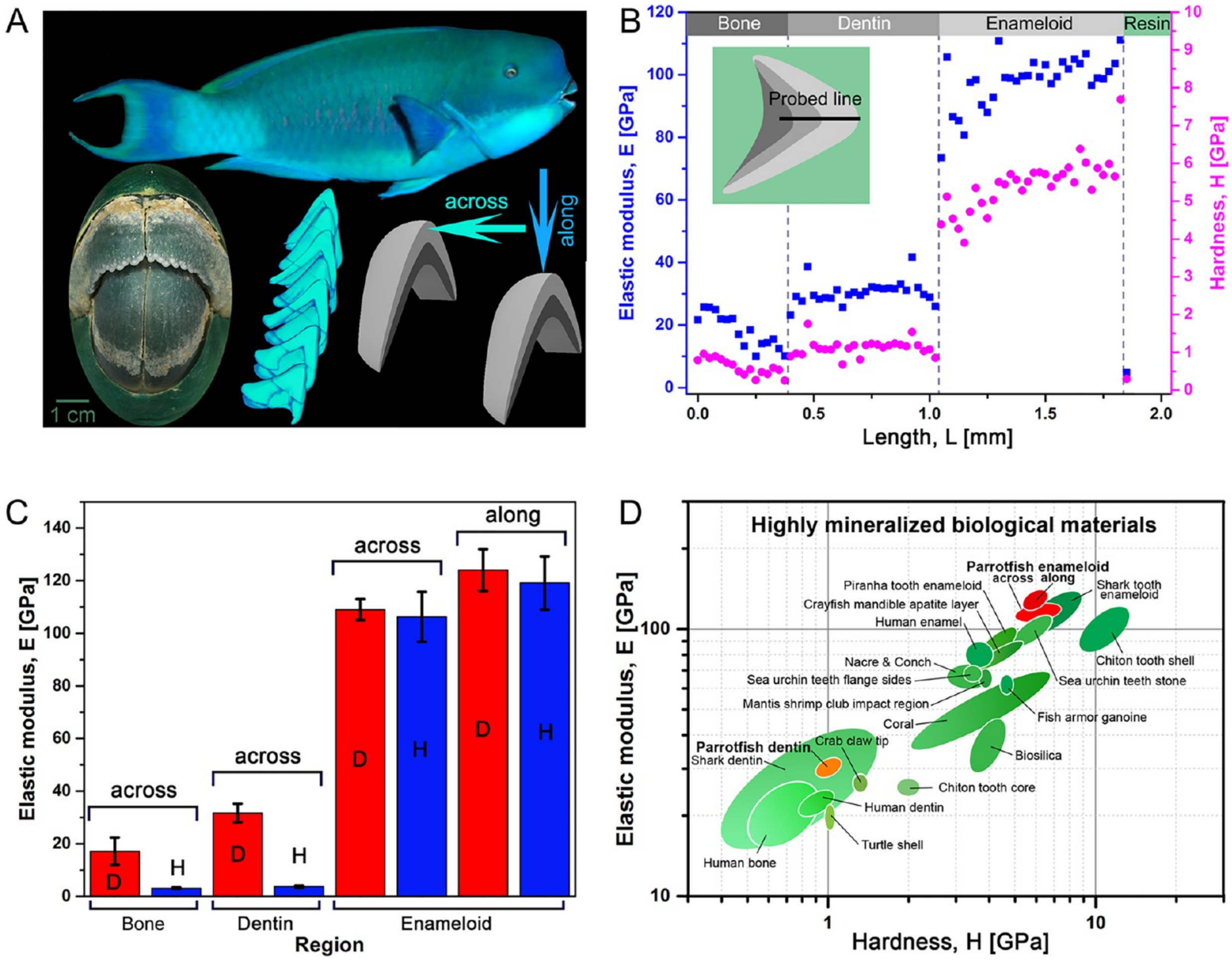

Figure 1. (A) Photograph of a steephead parrotfish *Chlorurus microrhinos* (top), which may grow up to 80 cm long. Its beak includes many teeth cemented together (lower left), and nine subsequent teeth in a series with the biting tooth at the top (tooth #1) are reconstructed with micro-CT. Arrows show the indentation directions across and along the biting direction. (B) Elastic modulus (E) and hardness (H) profiles measured on the "Probed line" on a parrotfish tooth #1, from the bone to the enameloid region. In parrotfish teeth, the pulp is replaced by bone as teeth mature, so bone backs dentin, which backs enameloid.[1] (C) Mean E values in the bone, dentin, and enameloid regions in both dry (D) and hydrated (H) conditions. (D) Ashby plot E *vs* H, including the present parrotfish tooth enameloid measured along and across the biting direction. Along the biting direction the parrotfish enameloid is one of the stiffest of all biominerals thus far analyzed, but not the hardest. It is less hard than the chiton (magnetite) or sea urchin (calcite) teeth, and, together with shark enameloid, harder than other vertebrate teeth. All other data were adapted from refs 2 and 3.

ones, each comprised of ~15 rows of teeth, continuously forming, surrounded by soft tissue at the forming end, and gradually becoming more mineralized and rigid as they mature and move toward the biting end of the beak, where the most mature biting tooth erupts from the bone tissue, which surrounds all other teeth. Figure 1 shows a complete beak, Figure S1 shows two such beaks in front and side views, and their resemblance to parrot beaks, whence the common name parrotfish. Figure S2 shows an example of a beak embedded in resin for mechanical and microscopic measurements. Figure 2 and Movie S1 show the microcomputed tomography (micro-CT) of the complex arrangement of subsequent teeth in one slice of a parrotfish beak. Figures S3 and S4 and Movie S2 show a model beak obtained by manually assembling 25 identical teeth in 3D to make them match experimental cross sections in 2D. This model reveals that teeth are rotated with respect to one another in a systematic pattern, thus producing the curvature of the beak.

What microscopic features contribute to the ability of the beak to bite off or scrape coral? To address this question, we

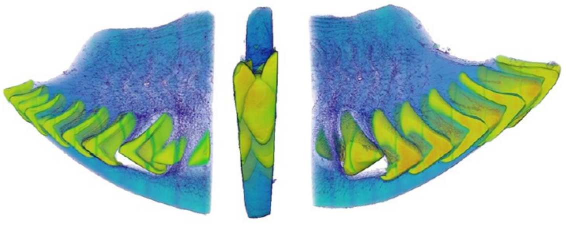

Figure 2. 3D volume rendering of a slice cut from 1/4 of a parrotfish beak specimen, generated from synchrotron micro-computed tomography (μCT) data. Denser enameloid is shown in yellow and green. The dentin behind each tooth, and the surrounding bone, which have similar densities, are shown in cyan and blue. The bottom dental plate of this parrotfish beak shows nine teeth with the most mature complete tooth and two partial ones erupting out of the blue bone tissue, at the left tip in the left panel, the top in the center, and the right in the right panel. This entire piece was 12.2 mm horizontally and 8.1 mm vertically. The pixel size is 3.25 μm both here and in Movie S1, which shows this same slice of beak rotating in space.

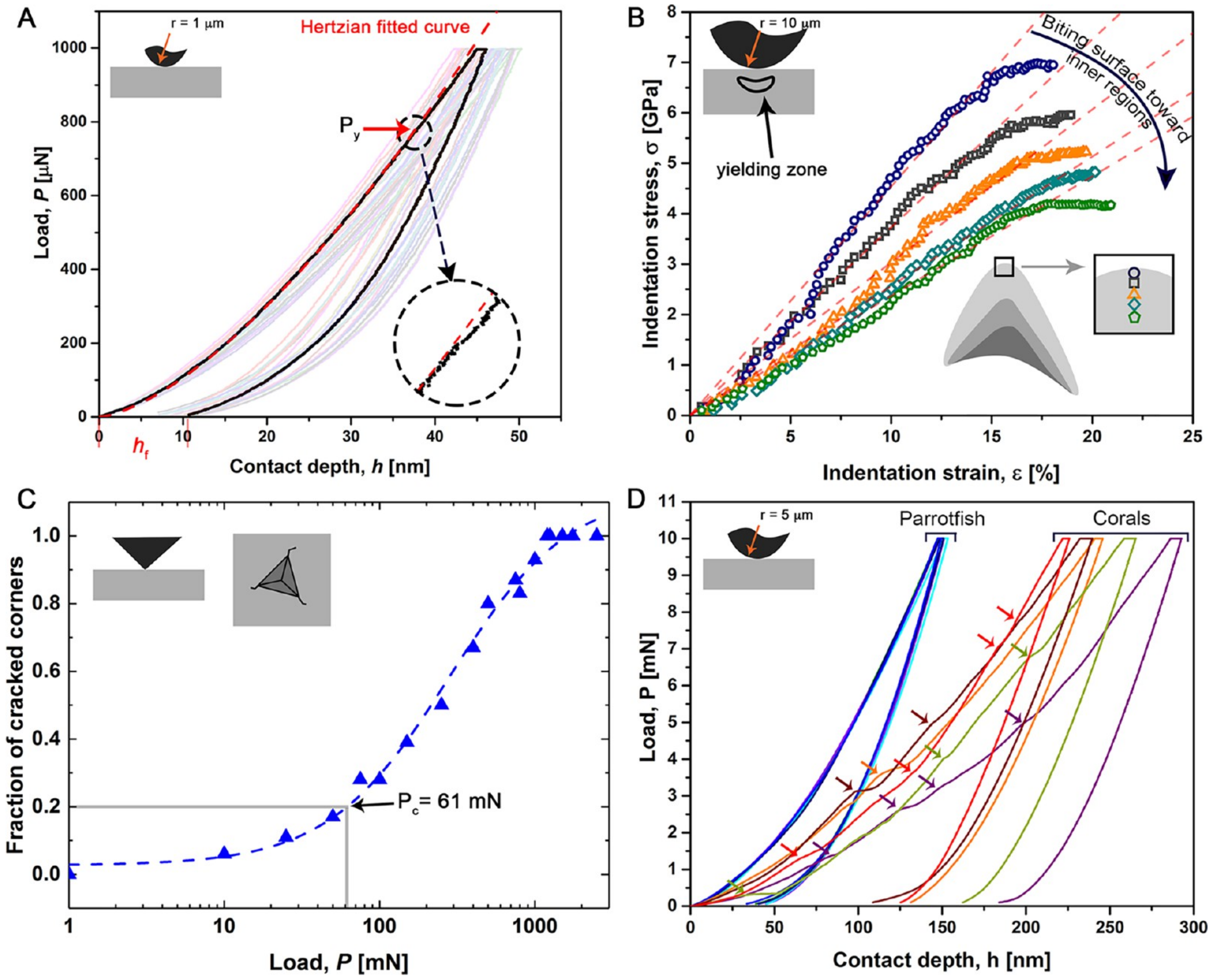

Figure 3. (A) Indentation curves obtained with a nominal 1 μm spherical (blunt) tip geometry. The red dashed line is the best fit to the Hertzian equation with $E = 124 \pm 8$ GPa, and deviation of the fit from the experimental curve denotes the load $P_y = 775$ μN at which yielding initiates for this test. In another test, P_y went up to 790 μN, but averaging the results of 11 tests we obtain 634 ± 123 μN (mean ± SD). (B) Indentation stress−strain curves obtained from the loading−unloading curves (shown in Figure S6) at incremental loads using a conospherical tip with 10 μm radius (indentation strain defined as a_c/R, where a_c is the contact radius and R the tip radius). At the biting surface of the teeth, the yield strength σ_y of enameloid is 6.7 GPa. (C) Fraction of cracked indent corners *vs* peak load using a cube-corner (sharp) tip geometry and a high-load (up to 10 N) transducer for the parrotfish tooth. The 20% cracking frequency is shown. (D) Indentation curves obtained with a 5 μm nominal spherical tip geometry on the parrotfish tooth and on a stony coral (*Porites lobata*). The colors in panel D only differentiate parrotfish curves (blue and cyan) from coral curves (all other colors). The arrows on the curves for the coral samples represent cracking events, detected at loads as low as 1 mN or less. No cracking was detected on the parrotfish tooth.

first measured the mechanical properties of polished sections of the beak of the steephead parrotfish *Chlorurus microrhinos*, using nanoindentation with both sharp and blunt contact geometries. Then we correlated structural and chemical analysis using scanning electron microscope energy dispersive X-ray analysis (SEM-EDX) and electron probe micro-analysis (EPMA), micro-Raman spectroscopy, photoelectron emission microscopy (PEEM) with polarization-dependent imaging contrast (PIC mapping), and X-ray microdiffraction.

Nanoindentation results on a transect of a parrotfish tooth are shown in Figure 1B, with data points acquired on a line through bone, dentin, and enameloid. The elastic modulus (E) measured across the biting direction in the enameloid increased from about 90 GPa at the dentin-enameloid junction to 105 GPa at the tip, thus the tooth is gradually stiffer toward the tip. A similar gradient in H and E was observed across all teeth measured, for example, those in Figures S5. This gradient cannot be an edge effect as described by Armitage *et al.*,[8] as the sharp Berkovich or cube-corner tips used to measure E and H have a radius of curvature of *ca.* 100 nm, which is orders of magnitude smaller than the 700 μm length over which the gradient is observed (Figure 1B). However, when the indentation was carried out along the biting direction, that is, with the indent at the distal tip of the tooth, pushing inward, the elastic modulus went up to 124 ± 8 GPa (Figure 1C). We note that the along:across direction ratio of E values is 1.18, matching the ratio of stiffness constants of the basal and prismatic crystal planes of fluorapatite (FAP) single crystals, 1.17, predicted by computer simulation.[9] The E values are comparable to those found for synthetic hydroxyapatite (HAP) or FAP,[10] which range from 100 GPa for HAP sintered at 1150 °C to 135 GPa for FAP sintered at 1250 °C, which is 98% dense, whereas the enameloid is only 85% dense FAP. A comparison with other biomaterials is shown on an elastic modulus (E) *vs* hardness (H) Ashby plot in Figure 1D. The parrotfish tooth enameloid along the biting direction is stiffer than almost any other biomineral measured, and across that direction it is comparable to the chiton tooth,[11] the sea urchin tooth,[12] and shark tooth enameloid.[3] Its hardness, which reaches 7.3 ± 0.4 GPa near the biting tip, is lower than those of chiton and sea urchin teeth, which are scrapers not biters, but greater than those of most other biters, including great white shark or piranha teeth,[13] but not other shark teeth.[3] Enamel from human molars is less stiff and hard than the parrotfish enameloid (95 and 3.5 GPa, respectively) and only in a thin layer at the surface do these figures increase to 120 and 6 GPa.[14] Similar stiffness and hardness of the parrotfish enameloid were found throughout the entire 1 mm thickness of the enameloid layer, with a slight gradient in both E and H in Figures 1B and S5B. Carr[15] found that the hardness of the pharyngeal teeth in parrotfish is comparable to that of human teeth.

In order for the fish teeth to be durable under their use condition (breaking coral), they must be resistant to abrasion. Abrasion is a complex process resulting from contact stresses between two solid bodies and involves damage by localized yielding and cracking as well as adhesion and decohesion. It also depends on the friction coefficient between the two materials and on the contact geometry, which can either be sharp or blunt.[2,16] Such complexity means that there is no single metric to characterize material performance against abrasion, thus requiring multiple parameter measurements, including yielding or cracking initiation under contact load. Against a blunt spherical abrasive tip, the mechanical contact behavior is initially elastic, then it enters the plastic regime (yielding) when the external load P exceeds a critical value P_y[16] that can be measured by fitting the initial portion of the load−displacement curve with the Hertzian equation, with P_y the load at which the experimental curve deviates from the Hertzian fit.[17] For a tip radius of 1 μm, we found an average P_y value of 634 ± 123 μN (n = 11) (Figure 3A), which significantly exceeds the value measured with identical nominal tip radius in the highly abrasion-resistant chiton tooth (P_y = 418 ± 60 μN).[2,11]

For a more complete assessment of abrasion resistance, we measured the indentation stress−strain curves using a blunt tip geometry and partial unloading/reloading cycles,[17] obtaining the partial loading/unloading curves shown in Figure S6. This method detects the elastic-to-plastic transition during contact loading and thereby provides the indentation yield strength σ_y, which represents a direct measure for the initiation of irreversible deformation occurring beneath the contact point. As shown in Figure 3B, we obtained σ_y = 6.7 GPa, which is more than 1 GPa greater than measured for the impact surface of the stomatopod dactyl club,[18] one of the most damage-tolerant biominerals thus far identified, and more than twice the indentation yield strength of human enamel, which is ∼3 GPa.[19] The σ_y = 6.7 GPa value approaches that of organic-free geologic FAP of 9.2 GPa,[18] thus indicating an extremely high resistance to yielding during contact loading.

Since resistance to contact can be viewed as a competition between yielding and cracking,[16,20] we also evaluated crack initiation against a sharp contact, using cube-corner geometry indentation at increasing loads,[21] and measured the fraction of indents with cracked corners.[22,23] Representative indentation fracture curves and post-indentation SEM images of indents are shown in Figure S7. The external load P_c at which cracks initiate from the indent corners provides a comparative metric to evaluate the resistance against contact cracking and can also be used to estimate the fracture toughness K_{Ic}.[23] The method is based on the concept that indentation cracks initiate above the threshold load P_c, leading to a relationship between P_c and K_{Ic}. However, the method also depends on the definition of cracking initiation, which was previously considered as the load corresponding to 50% cracking frequency (at 50% P_c is 213 mN for the parrotfish enameloid and 165 mN for the mantis shrimp club). Whereas the method is adequate to comparatively assess P_c of different brittle materials, it likely overestimates K_{Ic} because a significant amount (50%) of indentation cracks initiate below the median value. Thus, to be conservative, we used 20% cracking frequency (Figure 3C) as the threshold and obtained P_c = 61 mN, from which we calculated $K_{Ic} \approx 2.5$ MPa·m$^{1/2}$. Because this calculated K_{Ic} is subject to the definition employed for the cracking threshold, we consider it semi-quantitative. The $K_{Ic} \approx 2.5$ MPa·m$^{1/2}$ obtained from enameloid is greater than that of fluorapatite (K_{Ic} = 0.8 MPa·m$^{1/2}$)[24] or human enamel (K_{Ic} = 0.7−1.3 MPa·m$^{1/2}$).[25] Parrotfish enameloid is also likely to exhibit significant R-curve behavior as observed in human enamel,[26] but indentation fracture does not capture this phenomenon. Higher σ_y is usually accompanied by a decrease in toughness,[27] but this is not observed when comparing parrotfish enameloid and dactyl club: enameloid has a higher yield strength than the club,[22] and yet its fracture toughness is similar.

For a spherical geometry, a suitable dimensionless metric to assess whether a hard material will either initially absorb plastic energy or crack under contact loading is the brittleness index, I_B:[28]

$$I_B = \left(\frac{D}{A}\right)\left(\frac{H}{E}\right)\left(\frac{H}{K_{Ic}}\right)^2 R \tag{1}$$

where D and A are constants equal to 0.848 and 8.63 × 10^3, respectively, H is the hardness, E the elastic modulus, and R the contact radius. If $I_B > 1$ the contact response is brittle, whereas for $I_B < 1$, it is quasi-plastic, that is, energy-absorbing plastic yielding will precede or preclude brittle cracking. Alternatively, the critical radius R_c above which the response switches from quasi-plastic to brittle (namely $I_B = 1$) can be estimated. Using our measurements, we find that $R_c \sim 40$ mm. Since the parrotfish tooth radius of curvature is on the order of 0.25−1 mm, the implication is that plastic yielding almost always precedes cracking in the teeth during biting. We also evaluated the critical radius of hard corals (*Balanophyllia europaea*, $K_{Ic} \approx$ 0.55 MPa·m$^{1/2}$, $H \approx 5$ GPa, and $E \approx 77$ GPa)[29] and found $R_c \approx$ 0.85 mm, implying a brittle response when subjected to contact stresses since corals are typically larger than 1 mm and thus contact radii are well above 1 mm. In other words, when biting coral, parrotfish teeth exhibit a quasi-plastic response, and yielding occurs only if very high external contact loads are applied (owing to the high σ_y value), whereas corals fail by brittle contact. This prediction was corroborated by conducting indentation on hard corals with a spherical tip, which confirmed nucleation of cracking events at loads as low as 1 mN (Figure 3D). By comparison, no cracking was detected on the parrotfish tooth and only minimal yielding occurred as evidenced by the small residual indentation depth h_r = 30 nm after unloading. Clearly, having a higher fracture toughness ensures that the coral breaks, not the teeth. Finally, we conducted a nanowear assessment test by rubbing a 1 μm cono-spherical tip over a polished surface with a 500 μN normal load, and the results are shown in Figure S8. The average depth of the eroded area was

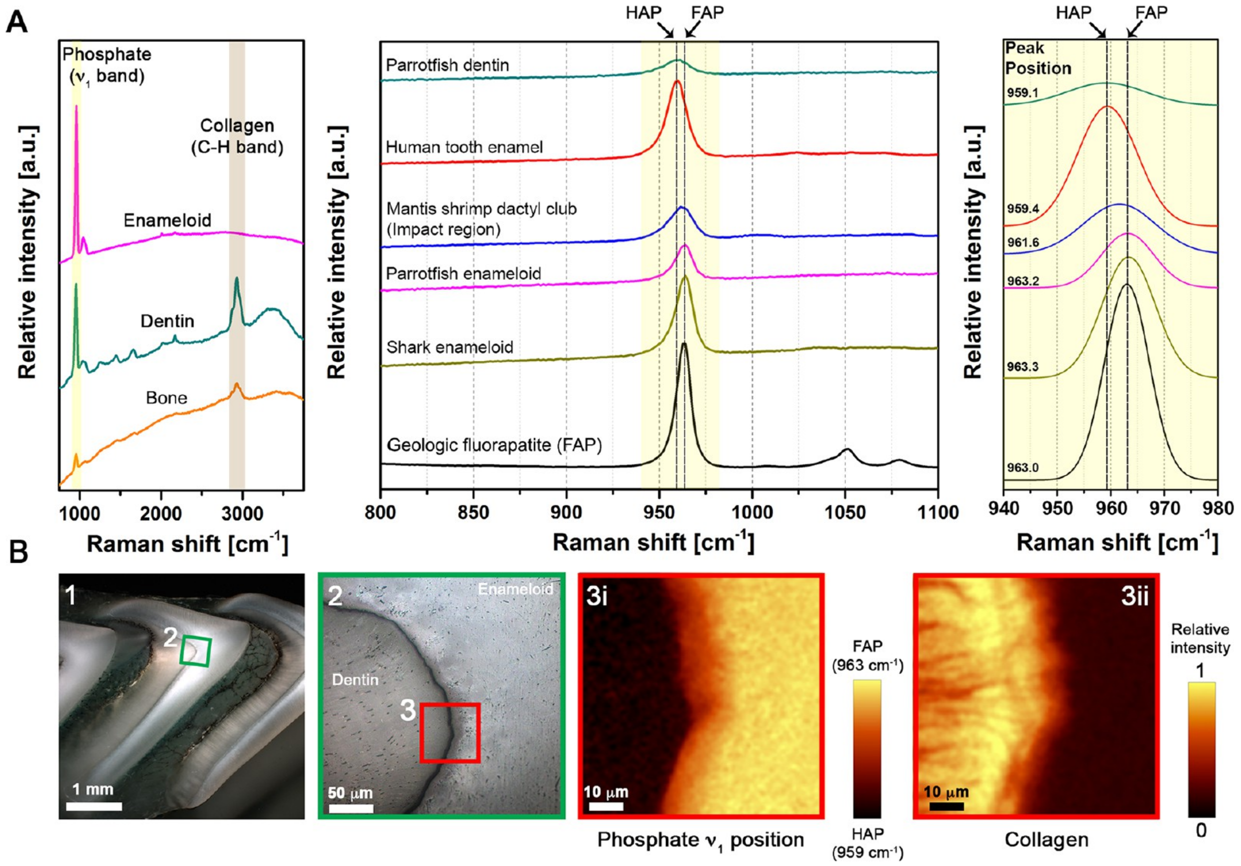

Figure 4. (A) Micro-Raman spectra of enameloid, dentin, and bone in parrotfish tooth (second row of teeth in the beak). Left: Broad-range Raman spectra showing that the collagen C−H band at ∼2800 cm^{-1} was only detected in bone and dentin regions, not in enameloid. Middle: Raman spectra of parrotfish enameloid and dentin, compared to human tooth enamel, shark enameloid, mantis shrimp dactyl club (impact region), and geologic FAP. The ν_1 phosphate band at ∼960 cm^{-1} is highlighted in yellow. Right: Zoom-in of the ν_1 band region, showing the shift between dentin and enameloid, related to the change in composition from HAP to FAP. (B) Optical micrographs and confocal Raman imaging of the dentin-enameloid junction. Panel 1 shows the overall tooth, and panel 2 is a zoom-in of the dentin-enameloid junction. The smaller subregion 3 indicated by the red square was used for Raman confocal imaging in panels 3i and 3ii, which represent maps of the ν_1 phosphate peak position and of the collagen C−H band intensity, respectively. Panel 3i illustrates the sharp transition from HAP to FAP at the dentin-enamel junction, and panel 3ii shows that no collagen was detected in the enameloid region.

50 nm, which is similar to that in the impact region of the mantis shrimp dactyl club, also shown in Figure S8, with no microcracks detected in the worn area, which is consistent with the quasi-plastic response.

Since nanomechanical data indicated that the parrotfish tooth and its enameloid, in particular, indeed exhibit great mechanical properties, we conducted a thorough chemical investigation, including composition and structure. Figure 4 shows micro-Raman data on the bone, dentin, and enameloid in each tooth forming the parrotfish beak. The dentin and bone exhibit a C−H band at around 2900 cm^{-1} consistent with collagen,[30] which is not detected in the enameloid. As with other vertebrate teeth, the mineral fraction is apatite. The position of the ν_1 phosphate band shifts from 962.1 to 965.6 cm^{-1} moving from dentin to enameloid, consistent with a change from HAP to FAP.[31] Within enameloid, the peak position is uniform. However, we cannot use this reading to pin down the exact composition because the frequency of the phosphate band also depends on substitutions other than F for OH, such as carbonation.[32] SEM-EDX (Figure S9) shows F in the enameloid and not in the dentin, confirming that the mineral in enameloid is FAP as has been found previously in parrotfish[33,34] and shark teeth.[3,35] EPMA along the transects in Figure S10 also confirms this mineral assignment (see Supporting Information).

The Ca L-edge X-ray absorption spectra from geologic FAP are presented in Figure 5 and show a dichroism, that is, a variation in spectral peak intensity depending on crystal orientation. This dichroism is much smaller than that in carbonates at the O or C K-edge, but still measurable, provided one ratios images acquired at two anticorrelated peaks (magnified in Figure 5) to maximize contrast, thus it can be used to effectively measure and display crystal orientations in PIC maps. PIC mapping has been used before for carbonate biominerals.[36−38] The apatite dichroism shown in Figure 5 is not limited to fish enameloid, but, if it is reproduced in hydroxyapatite, it could in principle be used in the future to PIC map the crystal orientations in teeth or bones of any animal, at the nano- and microscales. We note that the PIC maps presented here have 60 nm pixels, and 60 µm field of view, thus both the nano and microscales were explored with this method, but the main differences are observed at the microscale.

Figure 6 shows the locations in the parrotfish beak where all the PIC maps were acquired. Figure 7 shows a transect of three areas across the enameloid of tooth #1, which bit corals during the life of the animal, Figure 8 reproduces and confirms these results on tooth #2, which never bit, and Figure 9 shows the tips of teeth #1−4.

DOI: 10.1021/acsnano.7b05044
ACS Nano 2017, 11, 11856−11865

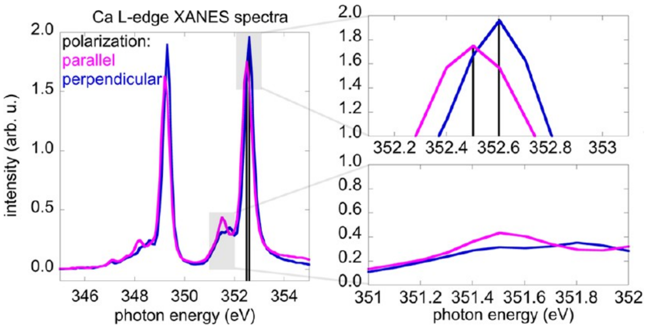

Figure 5. Calcium L-edge X-ray absorption near-edge structure (XANES) spectra were extracted from a 2.5 μm × 2.5 μm region, on the same crystal of geologic fluorapatite, and linearly polarized X-ray illumination either parallel or perpendicular to the crystalline *c*-axis. Parallel polarization maximizes the main peak indicated by the vertical black lines. The energy regions shaded in light gray are magnified on the right and show peaks at 352.6 and 351.6 eV, which exhibit the anticorrelated peak intensities termed dichroism. We acquired PEEM images at these two energies and used their ratio to obtain the PIC maps in Figures 6–9.

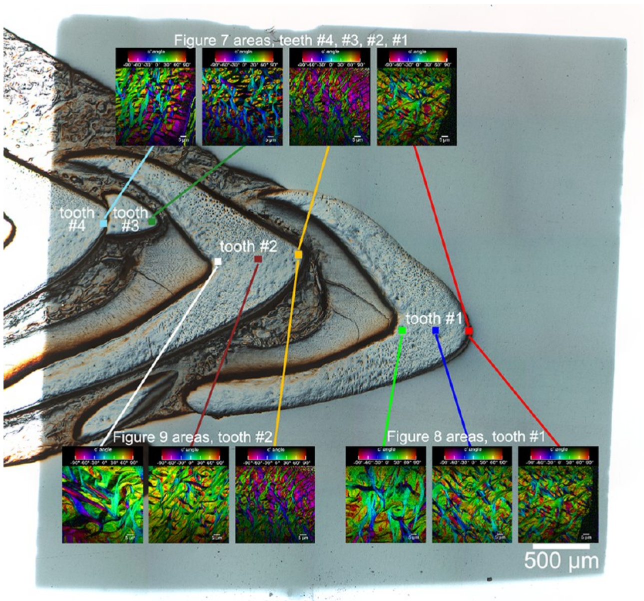

Figure 6. VLM micrograph of embedded and polished parrotfish teeth. The colored squares the 60 μm × 60 μm areas where the PIC maps of Figures 7–9 were acquired.

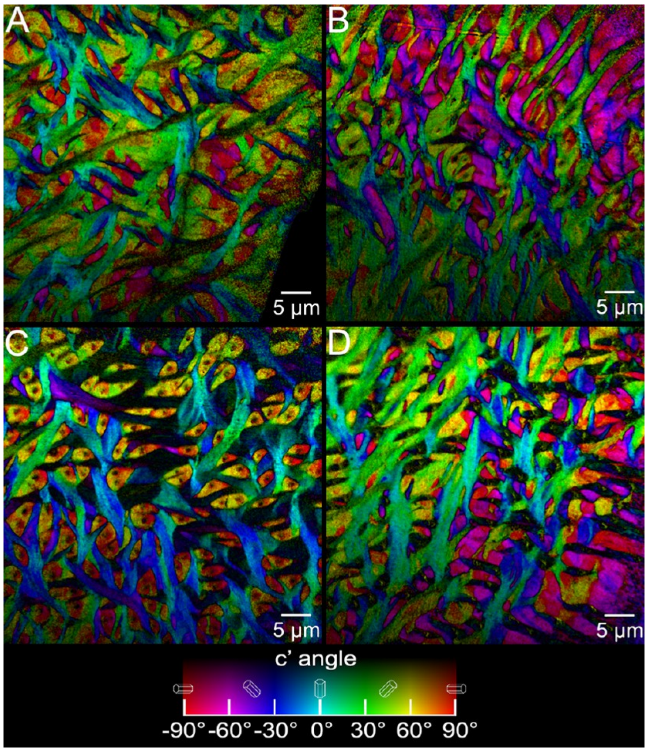

Figure 7. PIC maps showing different fluorapatite crystal sizes and orientations at the biting tips of teeth #1–4 as labeled in Figure 6. Two μm-wide fibers, made of 100 nm wide FAP crystals, are interwoven. The crystal orientations, shown schematically by prisms in the color bar, are as seen in projection perpendicular to the X-ray beam, which comes in from the right, at 30° from the surface.

In Figure 7 we present PIC maps acquired at the tips of four different teeth, consistently showing ∼2 μm fibers interwoven as the warp and the weave in fabric and running approximately 90° from each other.

In Figures 8 and 9 one can see a clear gradient in fiber diameter, varying from an average of 5 μm at the back to 2 μm at the biting tip of the tooth. In addition, the fiber orientations are anisotropic, which may be related to the anisotropy we observe for the elastic modulus along and across the biting tip (Figure 1). Another view of the fiber orientations in Figure 8 is presented in Figure S11, in which the *c*-axes at selected points are shown as vectors, superimposed on the same PIC map as in Figure 8 middle, and in Movie S3 the PIC map and vectors are rotated, thus the vector orientations are easier to see in 3D space. Unexpectedly, in a few fibers curving by 90° (arrows in Figure S11), the observed crystal orientations do not vary significantly. When the fibers run perpendicular to the polished surface of the sample, they invariably exhibit a dark dot at their center, as can be seen in Figure 7C. The vectors in Figure S12, shown in 3D in Movie S4, confirm that the fibers with black dots are indeed oriented nearly perpendicular to the image plane. Black in a PIC map indicates no polarization dependence, thus these can either be holes, amorphous minerals, or organics. We believe they are holes, as they are clearly visible in visible light microscope (VLM) as well. In this case they could be cell channels, as observed in sea urchin teeth.[39−41]

Fiber patterns similar to those in Figures 7–9 are seen in the fracture surfaces of Figure S13. These fracture surface patterns are in turn similar to those found previously for fish enameloids.[3,35,42] However, we do not see three well-defined layers, as found in sharks,[43] either by VLM, PEEM-PIC mapping, or SEM techniques (see Supporting Information).

X-ray microdiffraction in Figure S14 shows that enameloid is under uneven strain along the *c*-axis and that the coherence length in FAP crystals perpendicular to the *c*-axis is ∼100 nm, in excellent agreement with the 100 nm width of the nanocrystals observed in PIC maps and SEM micrographs in Figures S13 and S15. The coherence length along the *c*-axis exceeds 1 μm. XRD measurements on shark teeth[3] yielded values of 30–40 nm for the coherence length perpendicular to the *c*-axis and 52 nm along the *c*-axis. No reflections were found other than those generated by FAP crystals.

DOI: 10.1021/acsnano.7b05044
ACS Nano 2017, 11, 11856−11865

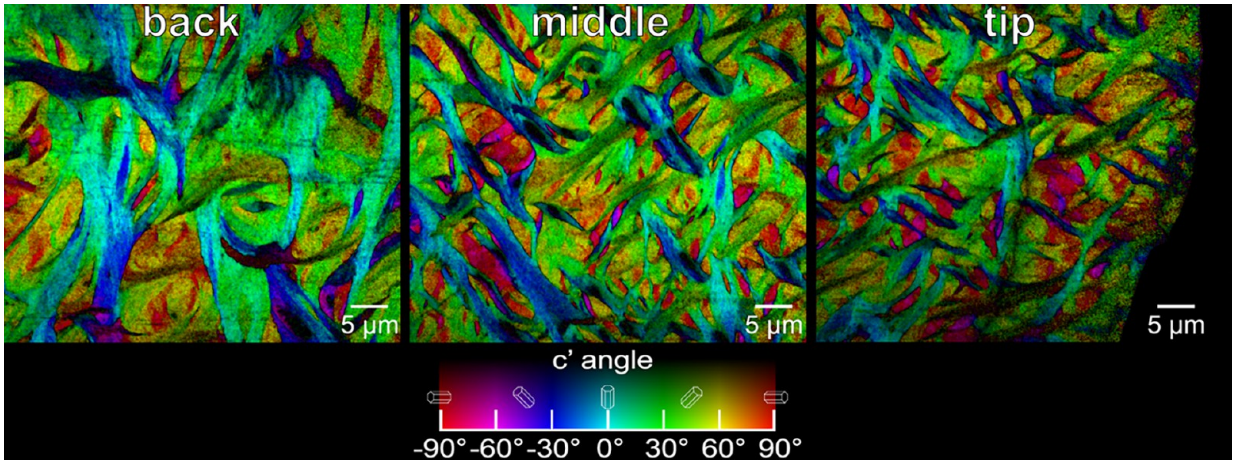

Figure 8. PIC maps showing the size and orientation of fibers at the back, the middle, and the tip of the enameloid layer of the biting tooth #1. Again, in all locations the fibers are made of 100 nm-wide, microns long FAP crystals, but the fiber average diameter varies gradually from 5 μm at the back of the tooth to 2 μm at the biting tip. See Figure 6 for the precise location of these areas.

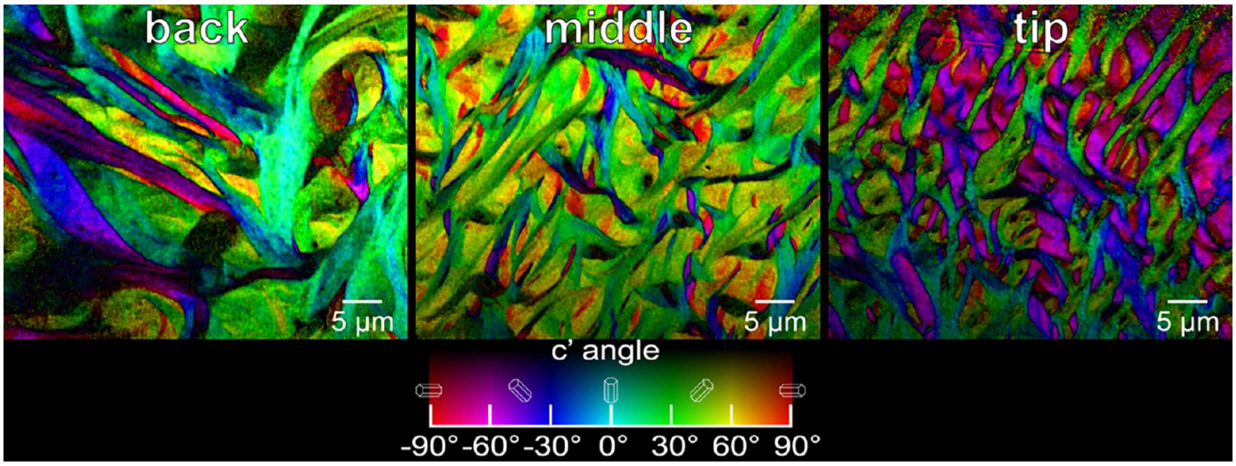

Figure 9. PIC maps as in Figure 8, but across tooth #2, which had not yet erupted when the animal was sacrificed and therefore had never bitten coral, whereas tooth #1 in Figure 8 had. See Figure 6 for the precise location of these areas.

Both the 100 nm nanostructure and the interwoven fiber microstructure must be at the origin of the observed toughness and resistance to wear.

X-ray microtomography (Figures 2 and S16–S18) shows that the density of the enameloid is 15% lower than that of geologic FAP. This density deficit relative to the geologic crystal makes it even more noteworthy that the elastic modulus of 124 GPa is so close to that of 98% dense synthetic sintered FAP (135 GPa).[10] However, it should be noted that Enax *et al.*[3] have reported values of 148–153 GPa and cite literature values of 143–150 GPa (geologic FAP)[44] and 126–135 GPa (synthetic HAP whiskers).[45] Raman, PIC maps, and SEM-BSE on polished sections do not reveal detectable areas of organics between the crystalline fibers in the mature tooth enameloid (Figures 7–9, 4A, and S15). If they exist, such organic interfaces could be smaller than the resolution of the current PIC maps (20 nm), as occurs in chiton teeth.[46,47] Figures S13 and S15 show that each crystalline fiber is in fact formed by a bundle of ~100 nm-wide elongated nanocrystals of FAP, approximately co-oriented. Thus, the structure appears to be compact and space-filling, analogous to the surface impact layer of the mantis shrimp club.[48] Absence of organics is consistent with the high values of hardness and stiffness measured, but the quasi-plastic response suggests that at least a very thin organic layer may be present to facilitate irreversible sliding of FAP nanocrystals as observed in parrotfish pharyngeal teeth[15] and the mantis shrimp dactyl club.[18] Also, that the fibers are made of small crystals, separated by organics, may allow the kind of strengthening discussed by Gao *et al.*[49] and the toughening described by Launey and Ritchie.[50]

DISCUSSION

The data shown here reveal the chemical composition and nano- and microstructure of parrotfish teeth, which confers on them fracture resistance and extreme wear tolerance.

The gradient in stiffness and hardness shown across the enameloid layer (Figure 1) cannot be due to the chemical composition, because that is constant across enameloid as shown by Raman, EDX, and EPMA. It cannot be due to the 100 nm-wide crystal nanostructure either, as that is constant in all locations of enameloid, forming (Figure S15), or fully formed and fractured (Figure S13). The fiber size gradient observed across the enameloid (Figures 8 and 9) is intriguingly correlated with the gradient in stiffness and hardness observed across the same transect (Figure 1). The direction of this gradient is interesting: both hardness and stiffness increase as the fiber diameter decreases. The increase in yield strength with decreasing grain size in nanostructured metals and alloys is well established,[51] and similar mechanisms may explain the increased hardness toward the tip. However, the increase in stiffness cannot be explained by the grain size, and the inverse correlation between stiffness and grain size remains unclear.

The observation in the microdiffraction data of Figure S14 of spatially varying lattice parameter at first sight conflicts with the uniform composition found by SEM-EDX and EPMA. However, it has been shown that, for instance, apatite fibers in human dentin have considerable compressive strain which varies according to the orientation of the fiber.[52] Internal strains have also been found in bone[53,54] and mollusk shells.[55,56] The observed compressive strain along the *c*-axis (fiber directions) in parrotfish teeth may add to their wear resistance by imposing closing stresses on microcracks nucleated near the surface of the tooth and thereby shielding microcracks from more deleterious tensile stresses,[20,56] although the mechanism by which organisms generate strain has not been elucidated.

The macrostructure of the dental plate may be relevant as well. Both parrotfish and sharks have multiple rows of teeth, such that the foremost teeth are used for a time, then are lost and replaced by successor teeth. The difference is that in parrotfish, the mature teeth are fused together and surrounded by bone to form a solid beak, as seen in Figures 1, 2, 6, S2−S4, S10, and S14, whereas in sharks, the teeth are separate from one another (*e.g.*, Figure 2 in Chen *et al.*[13]).

Each tooth at the biting surface is backed by those that will succeed it. Finally, the biting tip teeth are replaced on a regular basis. The conveyor belt of continuously forming teeth is reminiscent of that observed in sea urchin teeth, which self-sharpen by sloughing off the entire most mature plate at the biting tip.[39] In parrotfish, the entire tooth #1 is lost, and tooth #2, which is identically shaped, as a cusp, is exposed to the biting edge, thus it is clear that the parrotfish beak as a whole also self-sharpens.

CONCLUSIONS

The dental plates composing the parrotfish beak are adapted to their function in several ways. The hardness and stiffness increase toward the tip of each tooth, as the average fiber diameter decreases from 5 to 2 μm. The material of individual teeth is stiff and exhibits a quasi-plastic contact response with high yield strength, resulting in extremely high abrasion resistance, which may be connected with the spatial variation of crystal orientation and residual compressive strains. In addition, the stony coral skeletons the parrotfish bites are brittle, and the stark contrast in the contact mechanics response results in a much greater rate of wear damage in the coral.

The combination of all these mechanisms contributes to the specialized function that enables the parrotfish to feed, maintain the health of coral reefs, produce white sandy beaches, in addition to providing inspiration for the design of ultrahigh abrasion-resistant materials for microscopic moving parts.

The observed gradient in fiber microsize, correlated with the gradient in hardness and stiffness, is another example of graded microstructures, which have been shown to provide improved wear resistance,[57,58] compared to other homogeneously sized structures recently inspired by enamel.[59,60] Nacre has inspired more research[61−63] and biomimetic materials[64,65] than any other biomineral. Parrotfish tooth enameloid has an intriguingly complicated structure, and mechanically it is stiff, hard, tough, and abrasion resistant. By providing an alternate bioinspired design for tough and wear-resistant ceramic-based composites, parrotfish teeth may be the new nacre.

EXPERIMENTAL SECTION

Detailed experimental methods are described in the Supporting Information. Briefly, we used parrotfish beaks from *Chlorurus microrhinos*, embedded, polished, and coated as described in refs 2, 37, and 66−69 for PEEM, SEM, EPMA, and VLM experiments. We did spectroscopy and PIC mapping using PEEM as well as X-ray microdiffraction and X-ray microtomography at the Advanced Light Source (ALS, Berkeley, CA). All nanomechanical studies were conducted at Nanyang Technological University, including contact mechanics, indentation fracture, and nanowear measurements, which were all done with a depth-sensing nanoindenter using both sharp and blunt (Hertzian) tip geometries. Raman spectroscopy and confocal imaging were also done at NTU, with supplementary spectra acquired at ALS.

ASSOCIATED CONTENT

Ⓢ Supporting Information

The Supporting Information is available free of charge on the ACS Publications website at DOI: 10.1021/acsnano.7b05044.

Figures S1−S18 and detailed experimental methods (PDF)

Movie S1: micro-CT of the complex arrangement of subsequent teeth in one slice of a parrotfish beak (MOV)

Movie S2: A model beak obtained by manually assembling 25 identical teeth in 3D to make them match experimental cross-sections in 2D (AVI)

Movie S3: PIC map and vectors are rotated as in Figure 8 (AVI)

Movie S4: The vectors in Figure S12 shown in 3D (AVI)

AUTHOR INFORMATION

Corresponding Authors

*E-mail: mamarcus@lbl.gov.
*E-mail: pupa@physics.wisc.edu.

ORCID

Dilworth Y. Parkinson: 0000-0002-1817-0716
Ali Miserez: 0000-0003-0864-8170
Pupa U. P. A. Gilbert: 0000-0002-0139-2099

Author Contributions

[#]These two authors contributed equally to this work. The manuscript was written by P.G., M.A.M., A.M., and S.A., and the other authors contributed methods, data acquisition, and processing.

Notes

The authors declare no competing financial interest.
[∇]Previously publishing as Gelsomina De Stasio

ACKNOWLEDGMENTS

We thank Gilles Le Moullac and Mireille Chinain for their generous gift of four parrotfish beaks and their species identification. We thank Elia Beniash, Boaz Pokroy, and Tali Mass for reading the manuscript and suggesting improvements. P.G. acknowledges support from the U.S. Department of Energy, Office of Science, Office of Basic Energy Sciences, Chemical Sciences, Geosciences, and Biosciences Division, under award DE-FG02-07ER15899, NSF grant DMR-1603192. A.M. acknowledges support from the Singapore National Research Foundation (NRF) through an individual NRF Fellowship. PEEM (BL 11.0.1.1), microdiffraction (BL

12.3.2), and tomography (BL 8.3.2) experiments were done at the Advanced Light Source, which is supported by the Director, Office of Science, Office of Basic Energy Sciences, of the U.S. Department of Energy under contract no. DE-AC02-05CH11231.

REFERENCES

(1) Sire, J. Y.; Davit-Beal, T.; Delgado, S.; Van Der Heyden, C.; Huysseune, A. First-Generation Teeth in Nonmammalian Lineages: Evidence for a Conserved Ancestral Character? *Microsc. Res. Tech.* **2002**, *59*, 408−434.

(2) Amini, S.; Miserez, A. Wear and Abrasion Resistance Selection Maps of Biological Materials. *Acta Biomater.* **2013**, *9*, 7895−7907.

(3) Enax, J.; Prymak, O.; Raabe, D.; Epple, M. Structure, Composition, and Mechanical Properties of Shark Teeth. *J. Struct. Biol.* **2012**, *178*, 290−299.

(4) Rotjan, R. D.; Lewis, S. M. Impact of Coral Predators on Tropical Reefs. *Mar. Ecol.: Prog. Ser.* **2008**, *367*, 73−91.

(5) Perry, C. T.; Kench, P. S.; O'Leary, M.; Morgan, K.; Januchowski-Hartley, F. Linking Reef Ecology to Island Building: Parrotfish Identified as Major Producers of Island-Building Sediment in the Maldives. *Geology* **2015**, *43*, 503−506.

(6) Glynn, P. W.; Manzello, D. P., Bioerosion and Coral Reef Growth: A Dynamic Balance. In *Coral Reefs in the Anthropocene*; Birkeland, C., Ed. Springer: Dordrecht, 2015; pp 67−97.

(7) Cramer, K. L.; O'Dea, A.; Clark, T. R.; Zhao, J.-x.; Norris, R. D. Prehistorical and Historical Declines in Caribbean Coral Reef Accretion Rates Driven by Loss of Parrotfish. *Nat. Commun.* **2017**, *8*, 14160.

(8) Armitage, O. E.; Oyen, M. L. Indentation across Interfaces between Stiff and Compliant Tissues. *Acta Biomater.* **2017**, *56*, 36.

(9) Mkhonto, D.; de Leeuw, N. H. A Computer Modelling Study of the Effect of Water on the Surface Structure and Morphology of Fluorapatite: Introducing a $Ca_{10}(Po_4)_6F_2$ Potential Model. *J. Mater. Chem.* **2002**, *12*, 2633−2642.

(10) Gross, K. A.; Rodríguez-Lorenzo, L. M. Sintered Hydroxyfluorapatites. Part Ii: Mechanical Properties of Solid Solutions Determined by Microindentation. *Biomaterials* **2004**, *25*, 1385−1394.

(11) Weaver, J. C.; Wang, Q.; Miserez, A.; Tantuccio, A.; Stromberg, R.; Bozhilov, K. N.; Maxwell, P.; Nay, R.; Heier, S. T.; DiMasi, E. Analysis of an Ultra Hard Magnetic Biomineral in Chiton Radular Teeth. *Mater. Today* **2010**, *13*, 42−52.

(12) Ma, Y.; Cohen, S. R.; Addadi, L.; Weiner, S. Sea Urchin Tooth Design: An "All-Calcite" Polycrystalline Reinforced Fiber Composite for Grinding Rocks. *Adv. Mater.* **2008**, *20*, 1555−1559.

(13) Chen, P.-Y.; Schirer, J.; Simpson, A.; Nay, R.; Lin, Y.-S.; Yang, W.; Lopez, M. I.; Li, J.; Olevsky, E. A.; Meyers, M. A. Predation *Versus* Protection: Fish Teeth and Scales Evaluated by Nanoindentation. *J. Mater. Res.* **2012**, *27*, 100−112.

(14) Lawn, B. R.; Lee, J. J.-W.; Chai, H. Teeth: Among Nature's Most Durable Biocomposites. *Annu. Rev. Mater. Res.* **2010**, *40*, 55−75.

(15) Carr, A. G. Microstructure and Mechanical Properties of Parrotfish Pharyngeal Teeth. Doctoral Thesis, University of Queensland, Queensland Australia, 2003.

(16) Zok, F.; Miserez, A. Property Maps for Abrasion Resistance of Materials. *Acta Mater.* **2007**, *55*, 6365−6371.

(17) Schuh, C. A. Nanoindentation Studies of Materials. *Mater. Today* **2006**, *9*, 32−40.

(18) Amini, S.; Tadayon, M.; Idapalapati, S.; Miserez, A. The Role of Quasi-Plasticity in the Extreme Contact Damage Tolerance of the Stomatopod Dactyl Club. *Nat. Mater.* **2015**, *14*, 943−950.

(19) He, L. H.; Swain, M. V. Enamel—a "Metallic-Like" Deformable Biocomposite. *J. Dent.* **2007**, *35*, 431−437.

(20) Lawn, B. *Fracture of Brittle Solids*; Cambridge University Press: Cambridge, UK, 1993.

(21) Marshall, D. B.; Cook, R. F.; Padture, N. P.; Oyen, M. L.; Pajares, A.; Bradby, J. E.; Reimanis, I. E.; Tandon, R.; Page, T. F.; Pharr, G. M. The Compelling Case for Indentation as a Functional Exploratory and Characterization Tool. *J. Am. Ceram. Soc.* **2015**, *98*, 2671−2680.

(22) Amini, S.; Masic, A.; Bertinetti, L.; Teguh, J. S.; Herrin, J. S.; Zhu, X.; Su, H.; Miserez, A. Textured Fluorapatite Bonded to Calcium Sulphate Strengthen Stomatopod Raptorial Appendages. *Nat. Commun.* **2014**, *5*, 4187.

(23) Miserez, A.; Weaver, J. C.; Thurner, P. J.; Aizenberg, J.; Dauphin, Y.; Fratzl, P.; Morse, D. E.; Zok, F. W. Effects of Laminate Architecture on Fracture Resistance of Sponge Biosilica: Lessons from Nature. *Adv. Funct. Mater.* **2008**, *18*, 1241−1248.

(24) Broz, M. E.; Cook, R. F.; Whitney, D. L. Microhardness, Toughness, and Modulus of Mohs Scale Minerals. *Am. Mineral.* **2006**, *91*, 135−142.

(25) Meyers, M. A.; Chen, P.-Y.; Lin, A. Y.-M.; Seki, Y. Biological Materials: Structure and Mechanical Properties. *Prog. Mater. Sci.* **2008**, *53*, 1−206.

(26) Bajaj, D.; Arola, D. D. On the R-Curve Behavior of Human Tooth Enamel. *Biomaterials* **2009**, *30*, 4037−4046.

(27) Wegst, U. G.; Bai, H.; Saiz, E.; Tomsia, A. P.; Ritchie, R. O. Bioinspired Structural Materials. *Nat. Mater.* **2015**, *14*, 23−36.

(28) Rhee, Y. W.; Kim, H. W.; Deng, Y.; Lawn, B. R. Brittle Fracture *Versus* Quasi Plasticity in Ceramics: A Simple Predictive Index. *J. Am. Ceram. Soc.* **2001**, *84*, 561−565.

(29) Pasquini, L.; Molinari, A.; Fantazzini, P.; Dauphen, Y.; Cuif, J.-P.; Levy, O.; Dubinsky, Z.; Caroselli, E.; Prada, F.; Goffredo, S.; Di Giosia, M.; Reggi, M.; Falini, G. Isotropic Microscale Mechanical Properties of Coral Skeletons. *J. R. Soc., Interface* **2015**, *12*, 20150168.

(30) Karampas, I. A.; Orkoula, M. G.; Kontoyannis, C. G. A Quantitative Bioapatite/Collagen Calibration Method Using Raman Spectroscopy of Bone. *J. Biophotonics* **2013**, *6*, 573−586.

(31) Leroy, G.; Leroy, N.; Penel, G.; Rey, C.; Lafforgue, P.; Bres, E. Polarized Micro-Raman Study of Fluorapatite Single Crystals. *Appl. Spectrosc.* **2000**, *54*, 1521−1527.

(32) Antonakos, A.; Liarokapis, E.; Leventouri, T. Micro-Raman and Ftir Studies of Synthetic and Natural Apatites. *Biomaterials* **2007**, *28*, 3043−3054.

(33) Prostak, K. S.; Seifert, P. Enameloid Formation in Two Tetraodontiform Fish Species with High and Low Fluoride Contents in Enameloid. *Arch. Oral Biol.* **1993**, *38*, 1031−1044.

(34) LeGeros, R. Z.; Suga, S. Crystallographic Nature of Fluoride in Enameloids of Fish. *Calcif. Tissue Int.* **1980**, *32*, 169−174.

(35) Enax, J.; Janus, A. M.; Raabe, D.; Epple, M.; Fabritius, H.-O. Ultrastructural Organization and Micromechanical Properties of Shark Tooth Enameloid. *Acta Biomater.* **2014**, *10*, 3959−3968.

(36) DeVol, R. T.; Metzler, R. A.; Kabalah-Amitai, L.; Pokroy, B.; Politi, Y.; Gal, A.; Addadi, L.; Weiner, S.; Fernandez-Martinez, A.; Demichelis, R.; Gale, J. D.; Ihli, J.; Meldrum, F. C.; Blonsky, A. Z.; Killian, C. E.; Salling, C. B.; Young, A. T.; Marcus, M. A.; Scholl, A.; Doran, A.; Jenkins, C.; Bechtel, H. A.; Gilbert, P. U. P. A. Oxygen Spectroscopy and Polarization-Dependent Imaging Contrast (Pic)-Mapping of Calcium Carbonate Minerals and Biominerals. *J. Phys. Chem. B* **2014**, *118*, 8449−8457.

(37) Gilbert, P. U. P. A.; Bergmann, K. D.; Myers, C. E.; Marcus, M. A.; DeVol, R. T.; Sun, C.-Y.; Blonsky, A. Z.; Tamre, E.; Zhao, J.; Karan, E. A.; et al. Nacre Tablet Thickness Records Formation Temperature in Modern and Fossil Shells. *Earth Planet. Sci. Lett.* **2017**, *460*, 281−292.

(38) Gilbert, P. U. P. A.; Young, A.; Coppersmith, S. N. Measurement of C-Axis Angular Orientation in Calcite (Caco3) Nanocrystals Using X-Ray Absorption Spectroscopy. *Proc. Natl. Acad. Sci. U. S. A.* **2011**, *108*, 11350−11355.

(39) Killian, C. E.; Metzler, R. A.; Gong, Y.; Churchill, T. H.; Olson, I. C.; Trubetskoy, V.; Christensen, M. B.; Fournelle, J. H.; De Carlo, F.; Cohen, S.; Mahamid, J.; Wilt, F. H.; Scholl, A.; Young, A.; Doran, A.; Coppersmith, S. N.; Gilbert, P. U. P. A. Self-Sharpening Mechanism of the Sea Urchin Tooth. *Adv. Funct. Mater.* **2011**, *21*, 682−690.

(40) Killian, C. E.; Metzler, R. A.; Gong, Y. T.; Olson, I. C.; Aizenberg, J.; Politi, Y.; Wilt, F. H.; Scholl, A.; Young, A.; Doran, A.;

DOI: 10.1021/acsnano.7b05044
ACS Nano 2017, 11, 11856−11865

Kunz, M.; Tamura, N.; Coppersmith, S. N.; Gilbert, P. U. P. A. The Mechanism of Calcite Co-Orientation in the Sea Urchin Tooth. *J. Am. Chem. Soc.* **2009**, *131*, 18404−18409.

(41) Wang, R.; Addadi, L.; Weiner, S. Design Strategies of Sea Urchin Teeth: Structure, Composition and Micromechanical Relations to Function. *Philos. Trans. R. Soc., B* **1997**, *352*, 469−480.

(42) Carr, A.; Kemp, A.; Tibbetts, I.; Truss, R.; Drennan, J. Microstructure of Pharyngeal Tooth Enameloid in the Parrotfish Scarus Rivulatus (Pisces: Scaridae). *J. Microsc.* **2006**, *221*, 8−16.

(43) Gillis, J. A.; Donoghue, P. C. The Homology and Phylogeny of Chondrichthyan Tooth Enameloid. *J. Morphol.* **2007**, *268*, 33−49.

(44) Saber-Samandari, S.; Gross, K. A. Micromechanical Properties of Single Crystal Hydroxyapatite by Nanoindentation. *Acta Biomater.* **2009**, *5*, 2206−2212.

(45) Viswanath, B.; Raghavan, R.; Ramamurty, U.; Ravishankar, N. Mechanical Properties and Anisotropy in Hydroxyapatite Single Crystals. *Scr. Mater.* **2007**, *57*, 361−364.

(46) Gordon, L. M.; Joester, D. Nanoscale Chemical Tomography of Buried Organic-Inorganic Interfaces in the Chiton Tooth. *Nature* **2011**, *469*, 194−197.

(47) Lowenstam, H. Lepidocrocite, an Apatite Mineral, and Magnetite in Teeth of Chitons (Polyplacophora). *Science* **1967**, *156*, 1373−1375.

(48) Weaver, J. C.; Milliron, G. W.; Miserez, A.; Evans-Lutterodt, K.; Herrera, S.; Gallana, I.; Mershon, W. J.; Swanson, B.; Zavattieri, P.; DiMasi, E. The Stomatopod Dactyl Club: A Formidable Damage-Tolerant Biological Hammer. *Science* **2012**, *336*, 1275−1280.

(49) Gao, H.; Ji, B.; Jäger, I. L.; Arzt, E.; Fratzl, P. Materials Become Insensitive to Flaws at Nanoscale: Lessons from Nature. *Proc. Natl. Acad. Sci. U. S. A.* **2003**, *100*, 5597−5600.

(50) Launey, M. E.; Ritchie, R. O. On the Fracture Toughness of Advanced Materials. *Adv. Mater.* **2009**, *21*, 2103−2110.

(51) Meyers, M. A.; Mishra, A.; Benson, D. J. Mechanical Properties of Nanocrystalline Materials. *Prog. Mater. Sci.* **2006**, *51*, 427−556.

(52) Kay, M. I.; Young, R.; Posner, A. Crystal Structure of Hydroxyapatite. *Nature* **1964**, *204*, 1050.

(53) Forien, J.-B.; Fleck, C.; Cloetens, P.; Duda, G.; Fratzl, P.; Zolotoyabko, E.; Zaslansky, P. Compressive Residual Strains in Mineral Nanoparticles as a Possible Origin of Enhanced Crack Resistance in Human Tooth Dentin. *Nano Lett.* **2015**, *15*, 3729−3734.

(54) Hoo, R. P.; Fratzl, P.; Daniels, J. E.; Dunlop, J. W.; Honkimäki, V.; Hoffman, M. Cooperation of Length Scales and Orientations in the Deformation of Bovine Bone. *Acta Biomater.* **2011**, *7*, 2943−2951.

(55) Almer, J.; Stock, S. Micromechanical Response of Mineral and Collagen Phases in Bone. *J. Struct. Biol.* **2007**, *157*, 365−370.

(56) Pokroy, B.; Fitch, A. N.; Lee, P. L.; Quintana, J. P.; El'ad, N. C.; Zolotoyabko, E. Anisotropic Lattice Distortions in the Mollusk-Made Aragonite: A Widespread Phenomenon. *J. Struct. Biol.* **2006**, *153*, 145−150.

(57) Liu, Z.; Zhu, Y.; Jiao, D.; Weng, Z.; Zhang, Z.; Ritchie, R. O. Enhanced Protective Role in Materials with Gradient Structural Orientations: Lessons from Nature. *Acta Biomater.* **2016**, *44*, 31−40.

(58) Suresh, S.; Mortensen, A. *Fundamentals of Functionally Graded Materials*; The Institut of Materials Communications: London, 1998.

(59) Yeom, B.; Sain, T.; Lacevic, N.; Bukharina, D.; Cha, S.-H.; Waas, A. M.; Arruda, E. M.; Kotov, N. A. Abiotic Tooth Enamel. *Nature* **2017**, *543*, 95−98.

(60) Le Ferrand, H.; Bouville, F.; Niebel, T. P.; Studart, A. R. Magnetically Assisted Slip Casting of Bioinspired Heterogeneous Composites. *Nat. Mater.* **2015**, *14*, 1172−1179.

(61) DeVol, R. T.; Sun, C.-Y.; Marcus, M. A.; Coppersmith, S. N.; Myneni, S. C. B.; Gilbert, P. U. P. A. Nanoscale Transforming Mineral Phases in Fresh Nacre. *J. Am. Chem. Soc.* **2015**, *137*, 13325−13333.

(62) Olson, I. C.; Kozdon, R.; Valley, J. W.; Gilbert, P. U. P. A. Mollusk Shell Nacre Ultrastructure Correlates with Environmental Temperature and Pressure. *J. Am. Chem. Soc.* **2012**, *134*, 7351−7358.

(63) Gilbert, P. U. P. A.; Metzler, R. A.; Zhou, D.; Scholl, A.; Doran, A.; Young, A.; Kunz, M.; Tamura, N.; Coppersmith, S. N. Gradual Ordering in Red Abalone Nacre. *J. Am. Chem. Soc.* **2008**, *130*, 17519−17527.

(64) Shi, L. R.; Chen, K.; Du, R.; Bachmatiuk, A.; Rummeli, M. H.; Xie, K. W.; Huang, Y. Y.; Zhang, Y. F.; Liu, Z. F. Scalable Seashell-Based Chemical Vapor Deposition Growth of Three-Dimensional Graphene Foams for Oil-Water Separation. *J. Am. Chem. Soc.* **2016**, *138*, 6360−6363.

(65) Xu, G. F.; Yao, N.; Aksay, I. A.; Groves, J. T. Biomimetic Synthesis of Macroscopic-Scale Calcium Carbonate Thin Films. Evidence for a Multistep Assembly Process. *J. Am. Chem. Soc.* **1998**, *120*, 11977−11985.

(66) Gilbert, P. U. P. A., Photoemission Spectromicroscopy for the Biomineralogist. In *Biomineralization Sourcebook, Characterization of Biominerals and Biomimetic Materials*, DiMasi, E., Gower, L. B., Eds.; CRC Press: Boca Raton, FL, 2014; pp 135−151.

(67) Frazer, B. H.; Gilbert, B.; Sonderegger, B. R.; De Stasio, G. The Probing Depth of Total Electron Yield in the Sub Kev Range: Tey-Xas and X-Peem. *Surf. Sci.* **2003**, *537*, 161−167.

(68) De Stasio, G.; Rajesh, D.; Ford, J.; Daniels, M.; Erhardt, R.; Frazer, B.; Tyliszczak, T.; Gilles, M.; Conhaim, R.; Howard, S.; Fowler, J.; Esteve, F.; Mehta, M. Motexafin-Gadolinium Taken up *in Vitro* by at Least 90% of Glioblastoma Cell Nuclei. *Clin. Cancer Res.* **2006**, *12*, 206−213.

(69) Najman, M.; Kasrai, M.; Bancroft, G.; Frazer, B.; De Stasio, G. The Correlation of Microchemical Properties to Antiwear (Aw) Performance in Ashless Thiophosphate Oil Additives. *Tribol. Lett.* **2004**, *17*, 811−822.

DOI: 10.1021/acsnano.7b05044
ACS Nano 2017, 11, 11856−11865